

## Optical polarimetry and high-resolution spectroscopy of the Chamaeleon I dark cloud<sup>(\*)</sup>(<sup>\*\*</sup>)

E. COVINO<sup>(1)</sup>, B. E. PENPRASE<sup>(2)</sup>, E. PALAZZI<sup>(3)</sup>

L. TERRANEGRA<sup>(1)</sup> and H. E. SCHWARZ<sup>(4)</sup>

<sup>(1)</sup> *Osservatorio Astronomico di Capodimonte - Napoli, Italy*

<sup>(2)</sup> *Pomona College, Department of Physics and Astronomy - Claremont, CA 91711, USA*

<sup>(3)</sup> *Istituto TESRE/CNR - Bologna, Italy*

<sup>(4)</sup> *Nordic Optical Telescope, Apartado 474 - E-38700 Sta. Cruz de La Palma, Canarias, Spain*

(ricevuto il 5 Dicembre 1996; approvato il 27 Febbraio 1997)

**Summary.** — Magnitudes of linear polarization in the UBVRI bands have been measured for about 30 background stars in the direction of the Chamaeleon I dark cloud. In addition, high-resolution spectroscopic observations in the wavelength ranges of the atomic species Ca II and Ca I and of the molecular species CH and CH<sup>+</sup> have been performed towards the highly reddened and early-type stars selected from the polarimetry sample. The data have been used to study the magnetic-field structure, the relation between polarization and extinction, and the relation between molecular abundances and polarization properties in the cloud. In this contribution we present some of the results.

PACS 96.40 – Cosmic rays.

PACS 96.50.Dj – Interplanetary gas and dust (including gegenschein and zodiacal light).

PACS 01.30.Cc – Conference proceedings.

### 1. – Introduction

Magnetic fields play an important role on the evolution of interstellar clouds. In particular, the relationship between the field geometry and the cloud morphology may provide clues to the most likely scenarios of dark-cloud collapse and evolution.

The Chamaeleon dark cloud is one of the nearest active star formation regions ( $d \approx 120\text{--}150$  pc). Thanks to its very close distance and relatively high galactic latitude ( $b \approx -16^\circ$ ), this cloud is well suited for investigating the magnetic field (m.f.) geometry and its relationship with the cloud morphology and with the on-going star formation. In

---

(\*) Paper presented at the VII Cosmic Physics National Conference, Rimini, October 26-28, 1994.

(\*\*) Paper based on observations collected at the European Southern Observatory, La Silla, Chile.

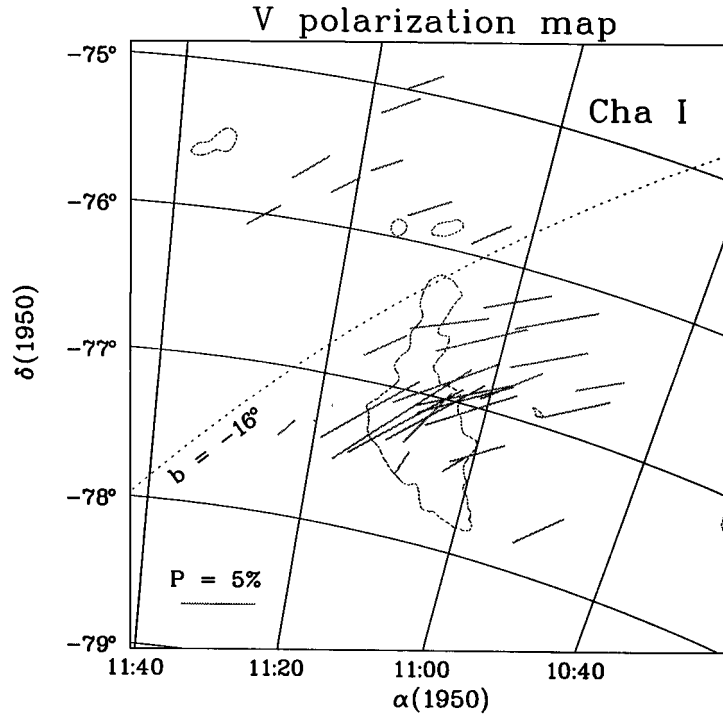


Fig. 1. – Average polarization vectors for polarimetric program stars. The  $100 \mu\text{m}$  contours of IRAS are also included. The length of the symbols is proportional to the percentage polarization.

addition, high-latitude clouds provide an important test of the role of extinction and m.f. on the chemical content and excitation state of molecules [1].

Measurements of optical linear polarization of starlight can be used to trace the geometry of the interstellar m.f. component,  $\vec{B}_\perp$ , in the plane of the sky. The observed polarization is produced by the (differential) extinction of non-spherical dust grains associated with the interstellar clouds along the line of sight. It is assumed, in fact, that elongated paramagnetic dust grains are aligned by the local interstellar m.f. via the Davis-Greenstein mechanism [2] with their short axes parallel to the field direction. Consequently, the extinction of starlight is more efficient in the direction perpendicular to the m.f., thus resulting in an observed polarization parallel to the m.f. direction.

A strong evidence that extinction by dust grains is responsible for the observed polarization comes from the existence of a correlation between the degree of polarization and the amount of reddening.

The wavelength dependence of the linear polarization can be usually expressed in the following normalized form, known as Serkowski's law [3]:

$$P(\lambda)/P_{\text{Max}} = \exp[-K \ln^2(\lambda_{\text{Max}}/\lambda)],$$

where  $\lambda_{\text{Max}}$  is the wavelength at which the maximum polarization,  $P_{\text{Max}}$ , is observed, and  $K \approx 1.15$ . The value of  $\lambda_{\text{Max}}$  normally falls in the range from  $0.35$  to  $0.9 \mu\text{m}$  and typically is found to be near  $0.55 \mu\text{m}$ . Larger values of  $\lambda_{\text{Max}}$  are expected in direction of dense clouds, indicating an increase in the mean grain size. A discussion of the theoretical arguments

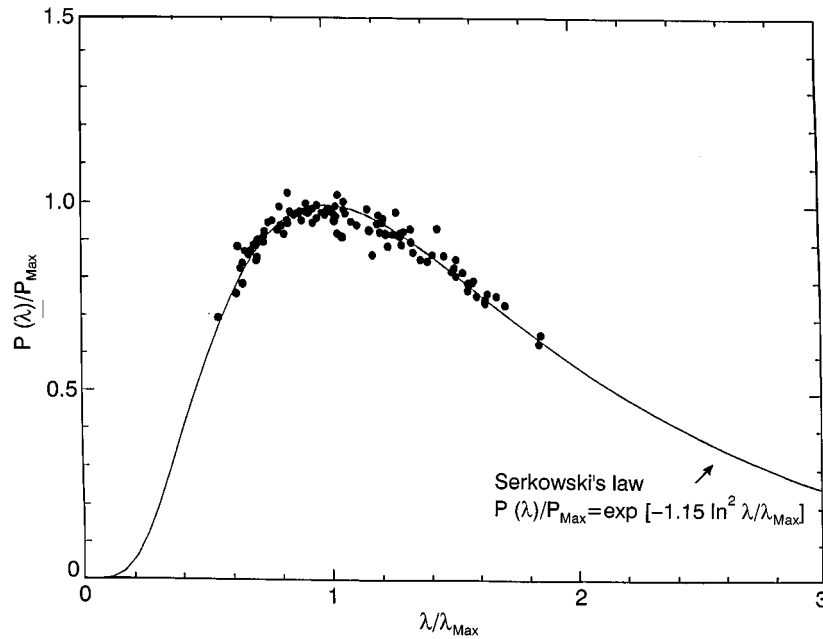


Fig. 2. – Least-square fit to Serkowski's law for selected stars. The Serkowski polarization model was fitted with  $K = 1.15$  and the free parameters  $P_{\text{Max}}$  and  $\lambda_{\text{Max}}$ .

behind the Serkowski polarization model may be found in Spitzer [2].

On the other hand, information on the chemistry in the cloud can be obtained from optical-absorption line studies of both atomic and molecular species. Observations of atomic species like Ca II and Ca I are used to derive characteristic densities of the cloud, while observations of molecular-absorption lines like CH and  $\text{CH}^+$  are used to probe the extent of warm, post-shock regions, since the formation of  $\text{CH}^+$  is thought to require an endothermic reaction which is more likely to occur in heated or shocked parts of the cloud.

## 2. – Observations

**2.1. Polarimetry.** – Some 30 background stars in the direction to Chamaeleon I dark cloud, from the list of the field stars presented by Whittet *et al.* [4], have been measured for linear polarization. The observations were obtained on five nights in March 1992 at ESO-La Silla using the 2.2 m telescope equipped with the PISCO polarimeter, in the  $\text{UBV(RI)}_C$  system.

**2.2. Spectroscopy.** – The background stars earlier than A0, suitable for the spectroscopic study of the cloud, were selected from the polarimetry sample. High-resolution spectroscopy observations were performed at the Coudé Auxiliary Telescope (CAT) at ESO during two observing runs in 1992 March and 1994 January. The data were obtained using a high-resolution CCD detector and the CES blue short camera. This instrument configuration provided a resolution,  $\lambda/\delta\lambda > 60\,000$  at the studied wavelengths.

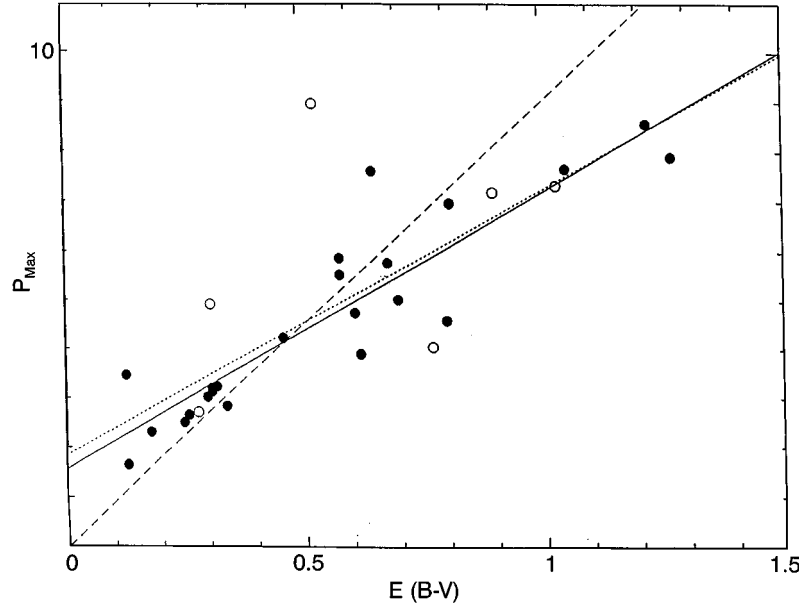


Fig. 3. – Maximum polarization,  $P_{\text{Max}}$ , plotted against  $E_{B-V}$  for the polarimetric sample. The filled circles indicate sightlines which had 5 measurements for fitting the Serkowski model, while the open circles are sightlines which only had measurements in 4 filters. The dotted line shows the best fit to all the points, and the solid line the best fit to sightlines which included 5 measurements. The dashed line represents the “maximum” polarization efficiency from [2].

### 3. – Results

The polarization map in the  $V$  band is presented in fig. 1.

It is noteworthy that the polarization vectors lie approximately in the direction parallel to the galactic plane and nearly perpendicular to the long axis of the dark cloud. This is fairly consistent with the view of a cloud collapse occurring along the magnetic-field lines. Our observations are also in very good agreement with those by McGregor *et al.* [5].

For selected stars we have fitted the percentage polarization with a Serkowski polarization model to derive values of  $\lambda_{\text{Max}}$  and  $P_{\text{Max}}$ . The data points, and their best fit are presented in fig. 2. The Serkowski model was fitted only to those stars which had accurate polarization measurements in at least four passbands. We excluded measurements from our fit which had polarization uncertainties  $P_{\lambda} > 1.6\%$ .

As shown in fig. 3, more heavily reddened stars also present, as expected, a higher degree of optical polarization. Also shown in fig. 3 are separate fits for the sight lines where 4 or 5 filter measurements were used to fit the data to the Serkowski model. For some of the stars the polarization to reddening ratio,  $P_{\text{Max}}/E_{B-V}$ , is very close to or even higher than the maximum polarization efficiency of  $0.09 \text{ mag}^{-1}$  [2].

All the stars observed through the densest part of the cloud have been identified with the ones which suffer higher extinction and polarization. These findings clearly indicate that the mean grain size tend to be larger in the denser parts of the cloud. In addition to that, a change in the grain size distribution along line of sights passing through the densest part of the cloud is also consistent with previous reports of an anomalously high visual-to-selective extinction ratio, ( $R \approx 5$ ) in the surroundings of Ced 111. Thus, this also

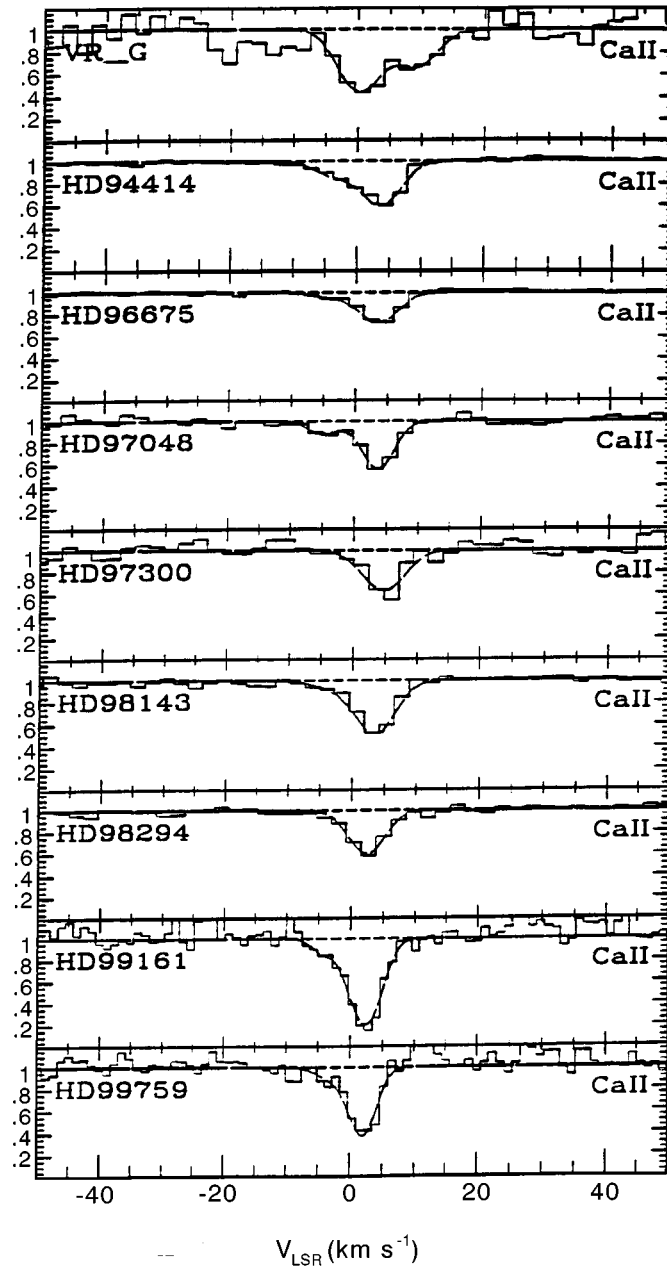


Fig. 4. – Spectra for all of our spectroscopic program stars in Ca II absorption, in order of right ascension. The Cha I cloud Ca II absorption appears at a nearly constant velocity of  $v_{\text{lsr}} = 4.5 \text{ km s}^{-1}$ , with a second blended component visible in sightlines at either end of the cloud.

TABLE I. – *Spectroscopic results.*

Star	$b_{\text{CaII}}$ (km s <sup>-1</sup> )	$N_{\text{CaII}}$ (cm <sup>-2</sup> )	$V_{\text{lsrCaII}}$ (km s <sup>-1</sup> )	$W_{\text{CaII}}$ (Å)	$b_{\text{CH}}$ (km s <sup>-1</sup> )	$N_{\text{CH}}$ (cm <sup>-2</sup> )	$V_{\text{lsrCH}}$ (km s <sup>-1</sup> )	$W_{\text{CH}}$ (Å)
VRg	3.13	$4.68 \cdot 10^{11}$	8.66	0.0514	–	–	–	–
VRg	3.12	$1.01 \cdot 10^{12}$	–0.38	0.0724	–	–	–	–
HD94414	2.10	$6.85 \cdot 10^{11}$	4.80	0.0383	1.16	$4.52 \cdot 10^{13}$	4.35	0.0247
HD94414	1.80	$1.55 \cdot 10^{11}$	–2.88	0.0120	–	–	–	–
HD96675	1.90	$4.03 \cdot 10^{11}$	4.58	0.0252	0.86	$3.13 \cdot 10^{13}$	3.74	0.0187
HD96675	1.80	$4.9 \cdot 10^{10}$	–3.72	0.0054	–	–	–	–
HD97048	1.67	$6.67 \cdot 10^{11}$	–7.751	0.0573	1.069	$3.435 \cdot 10^{13}$	4.28	0.0180
HD97300	1.51	$8.11 \cdot 10^{11}$	4.16	0.0392	1.60	$1.74 \cdot 10^{13}$	4.63	0.0112
HD98143	1.90	$1.02 \cdot 10^{12}$	4.65	0.0398	0.61	$8.05 \cdot 10^{12}$	7.52	0.0051
HD98143	1.80	$9.95 \cdot 10^{12}$	–2.88	0.0102	–	–	–	–
HD98294	2.09	$5.61 \cdot 10^{11}$	1.81	0.0386	0.76	$1.34 \cdot 10^{13}$	2.88	0.0080
HD98561	–	–	–	–	0.74	$1.14 \cdot 10^{13}$	2.67	0.0068
HD99161	2.24	$1.55 \cdot 10^{12}$	2.03	0.074	0.71	$5.48 \cdot 10^{12}$	3.49	0.0036
HD99161	1.05	$9.59 \cdot 10^{10}$	–4.52	0.0087	–	–	–	–
HD99759	1.55	$8.46 \cdot 10^{11}$	1.72	0.051	0.90	$2.98 \cdot 10^{13}$	3.18	0.0177
HD99759	2.60	$1.04 \cdot 10^{11}$	–2.76	0.0077	–	–	–	–

Star	$b_{\text{CaI}}$ (km s <sup>-1</sup> )	$N_{\text{CaI}}$ (cm <sup>-2</sup> )	$V_{\text{lsrCaI}}$ (km s <sup>-1</sup> )	$W_{\text{CaI}}$ (Å)	$b_{\text{CH}^+}$ (km s <sup>-1</sup> )	$N_{\text{CH}^+}$ (cm <sup>-2</sup> )	$V_{\text{lsrCH}^+}$ (km s <sup>-1</sup> )	$W_{\text{CH}^+}$ (Å)
VRg	–	–	–	–	–	–	–	–
VRg	–	–	–	–	–	–	–	–
HD94414	–	$< 1.47 \cdot 10^{10}$	–	$< 0.0041$	1.00	$5.58 \cdot 10^{13}$	2.69	0.0240
HD96675	–	$< 4.71 \cdot 10^9$	–	$< 0.0013$	–	$< 3.20 \cdot 10^{12}$	–	$< 0.0028$
HD97048	–	$< 1.95 \cdot 10^9$	–	$< 0.0036$	–	$< 1.50 \cdot 10^{12}$	–	$< 0.0013$
HD97300	–	$< 1.42 \cdot 10^9$	–	$< 0.0026$	1.06	$1.46 \cdot 10^{11}$	0.84	$< 0.0001$
HD97300	–	–	–	–	1.04	$3.34 \cdot 10^{12}$	2.59	$< 0.0030$
HD98143	–	$< 2.90 \cdot 10^{10}$	–	$< 0.0080$	–	$< 7.65 \cdot 10^{12}$	–	$< 0.0068$
HD98294	–	$< 1.46 \cdot 10^{10}$	–	$< 0.0040$	–	$< 6.83 \cdot 10^{12}$	–	$< 0.0060$
HD98561	–	–	–	–	–	–	–	–
HD99161	–	$< 1.70 \cdot 10^{10}$	–	$< 0.0047$	–	$< 1.38 \cdot 10^{13}$	–	$< 0.0121$
HD99759	–	$< 1.17 \cdot 10^{10}$	–	$< 0.0032$	2.00	$1.88 \cdot 10^{13}$	0.31	0.0167

provides further support to the suggestion that the distance to the Cha I dark cloud is not larger than about 160 pc [6].

Table I lists the derived line fit parameters at each observed wavelength for the stars observed spectroscopically:  $V_{\text{lsr}}$ , the radial velocity of the cloud in the Local Standard of Rest,  $b$ , the velocity width,  $W_{\lambda}$ , the equivalent width, and  $N$ , the column density.

Figure 4 shows the CaII K spectra for some of the observed stars on a velocity scale. From both the table and the figure it is apparent that for most clouds the CaII absorption is dominated by one strong component whose detailed structure is obscured by saturation and/or line blending over a spectral range corresponding to 2–4 km s<sup>-1</sup>.

One remarkable aspect of the only CH<sup>+</sup> detection (HD99759) is the velocity offset from

the CH measurements. This behaviour is not uncommon for CH<sup>+</sup> and is consistent with the predicted offset from shock formation models [7].

The derived CH column densities have been compared with the measurements towards standard dark-cloud sightlines [8, 9]. It results that some of them (*e.g.*, HD94414, HD96675 and HD99759) are molecular-rich lines of sight. This indicates that some physical process is causing either an increased production of molecular species, or a decreased photoionization of molecular species, or an anomalous extinction for a given value of  $E(B - V)$ , or some combination of these.

#### REFERENCES

- [1] PENPRASE B. E., *Astrophys. J. Suppl. Ser.*, **88** (1993) 433.
- [2] SPITZER L., *Physical Processes in the Interstellar Medium* (Wiley, New York) 1978, p. 187.
- [3] COYNE G. V., GEHRELS S. J. T. and SERKOWSKI K., *Astron. J.*, **79** (1974) 581.
- [4] WHITTET D. C. B., KIRrane T. M., KILKENNY D., OATES A. P., WATSON F. G. and KING D. J., *Mon. Not. R. Astron. Soc.*, **224** (1987) 497.
- [5] MCGREGOR P. J., HARRISON T. E., HOUGH J. H. and BAILEY J. A., *Mon. Not. R. Astron. Soc.*, **267** (1994) 755.
- [6] SCHWARTZ R. D., in *Low Mass Star Formation in Southern Molecular Clouds* ESO Scientific Report No. 11, edited by BO REIPURTH (1991), p. 93.
- [7] DRAINE B. T. and KATZ N., *Astrophys. J.*, **306** (1986) 655.
- [8] DANKS A. C., FEDERMAN S. R., LAMBERT D. L., *Astron. Astrophys.*, **130** (1984) 62.
- [9] DANKS A. C., PENPRASE B. E., CRANE P. and PALAZZI E., unpublished (1990).